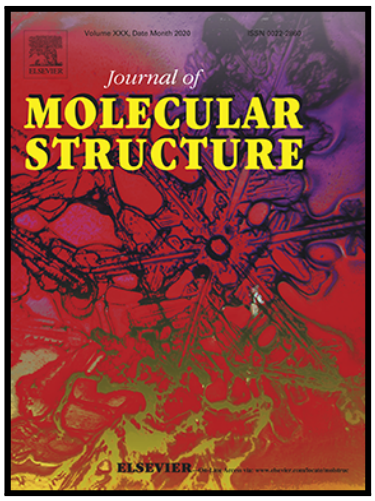

Exploration of synthesis, structural aspects, DFT studies and bio-efficacy of some new DHA-benzohydrazide based copper(II) complexes

Richa , Sunil Kumar , Jayant Sindhu , Poonam Choudhary , Sundeep Jaglan , Ennio Zangrando , Rakesh Kumar , Subash C. Sahoo , Vinod Kumar , Surinder K. Mehta , Ramesh Kataria

PII: S0022-2860(20)31775-0
DOI: https://doi.org/10.1016/j.molstruc.2020.129460
Reference: MOLSTR 129460

To appear in: *Journal of Molecular Structure*

Received date: 18 August 2020
Revised date: 13 October 2020
Accepted date: 14 October 2020

Please cite this article as: Richa , Sunil Kumar , Jayant Sindhu , Poonam Choudhary , Sundeep Jaglan , Ennio Zangrando , Rakesh Kumar , Subash C. Sahoo , Vinod Kumar , Surinder K. Mehta , Ramesh Kataria , Exploration of synthesis, structural aspects, DFT studies and bio-efficacy of some new DHA-benzohydrazide based copper(II) complexes, *Journal of Molecular Structure* (2020), doi: https://doi.org/10.1016/j.molstruc.2020.129460

Highlights

- Solvent coordinated Cu(II) complexes (**5a-5g**) have been synthesized and characterized by X-ray diffraction analysis.
- Copper is tetra-coordinated by chelating carbohydrazide ligand and coordinated solvent.
- The intermolecular interactions revealed the importance of O-H interactions in self-assembly and the higher chemical stability of **5c** was established by DFT studies.
- Compound **5f** shows potent antibacterial activity against *B*. *subtilis* with MIC and MBC value of 32 μM.

Exploration of synthesis, structural aspects, DFT studies and bio-efficacy of some new DHA-benzohydrazide based copper(II) complexes

Richa[a], Sunil Kumar[b], Jayant Sindhu[c], Poonam Choudhary[d], Sundeep Jaglan[d], Ennio Zangrando[e], Rakesh Kumar[a], Subash C. Sahoo[a], Vinod Kumar [f], Surinder K. Mehta [a], Ramesh Kataria[a]*

[a]Department of Chemistry and Centre for Advance Studies in Chemistry, Panjab University, Chandigarh-160014, India

[b]Department of Chemistry, School of Basic and Applied Sciences, Maharaja Agrasen University, Baddi, Solan-174103, India

[c]Department of Chemistry, COBS & H, CCS Haryana Agricultural University, Hisar-125004, India

[d]Microbial Biotechnology Division, CSIR-Indian Institute of Integrative Medicine, Canal Road, Jammu-180001, India

[e]Department of Chemical and Pharmaceutical Sciences, University of Trieste, Trieste 34127, Italy

[f]Department of Chemistry, C. U. Haryana, Mahendergarh-123031, India

Email: rkataria@pu.ac.in

ABSTRACT

A copper (II) complex with ligand obtained by the dehydrative condensation of 3-acetyl-6-methyl-2*H*-pyran-2,4(3*H*)-dione (DHA) and benzohydrazide has been synthesized. The complex species are additionally coordinated by various solvent molecules, namely ethanolamine, methanol, DMF, dimethyl amine, isopropyl amine, diisobutylamine, and ethylenediamine (5**a-5g**) have been synthesized. All the complexes were characterized by single crystal X-ray diffraction analysis and other analytical techniques. In each case, the copper atom is tetra-coordinated by chelating carbohydrazide ligand through *O*, *N*, *O* donor atoms and the *N/O* heteroatom from the coordinated solvent (except for ethylenediamine, where Cu is pentacoordinated). The intermolecular interactions present in each complex have been quantified using Hirshfeld surface analysis, and the electrostatic properties associated with these complexes were calculated using DFT studies. Considering the expected bioactivity of carbohydrazide derivatives, the antibacterial activity of ligand and copper complexes was tested against pathogenic Gram-positive and Gram-negative bacteria using ciprofloxacin as positive control. Compound **4** and **5f** shows potent antibacterial activity against *B. subtilis* with MIC and MBC value of 32 μM

Keywords: Antibacterial, Copper complex, Carbohydrazide, DFT, X-ray crystal structure

1 INTRODUCTION

Design and synthesis of bioinorganic compounds of biological interest has attracted considerable interest in past few years. The pharmacokinetic and pharmacodynamic properties of an agent are dependent upon solubility and bio-availability, which can be significantly enhanced by complexation. [1,2] It has been well evident in the literature that the bioactivity of metal complexes surpasses organic ligands. Choosing proper ligand and its chelation with suitable metal complex are some of the key factors for controlling the biological

efficacy of compounds. Copper complexes have also been explored as catalyst in asymmetric photoredox reactions [3], hydroalkylation of alkynes [4], alcohol oxidation [5] and C-H activation in the Henry reaction [6]. In addition, many sensing applications have utilized copper complexes for the detection of hydrogen peroxide and nitrite [7], adrafinil [8] and dissolved oxygen in water.[9] In addition to this a wide range of biological activity has been associated with copper complexes [10–12] which have attracted scientific community to develop novel, selective and less toxic copper compounds with promising biological properties.

Similarly, pyrones consist of a diverse group of bioactive metabolites, *viz.* cytotoxic, antialgal, antibacterial, and antifungal activity.[13–16] Recently, Marc Stadler and his coworkers isolated new α-pyrone derivatives **(Ia-Ib)**, udagawanones A and B, isolated from cultures of the endophyte *Neurosporaudagawae*, which were moderately active against fungi and mammalian cells[17]. Li *et al.* isolated two new Pleospyrones analogues (chlamydosporol derivatives) from the culture of the endophytic fungus *Pleosporales sp.* Sigrf05. [18] These analogues (**IIa** and **IIb**) exhibited good cytotoxicities against various cancer cell lines. Analogues of Maltol, a natural product that exhibits *in vitro* antiproliferative activity against cancer cell lines have been synthesized [19,20]. A copper complex (**III**) of Maltol a natural product exhibits *in vitro* antineoplastic activity against HeLa cell lines when performed using MTT assay. [21]

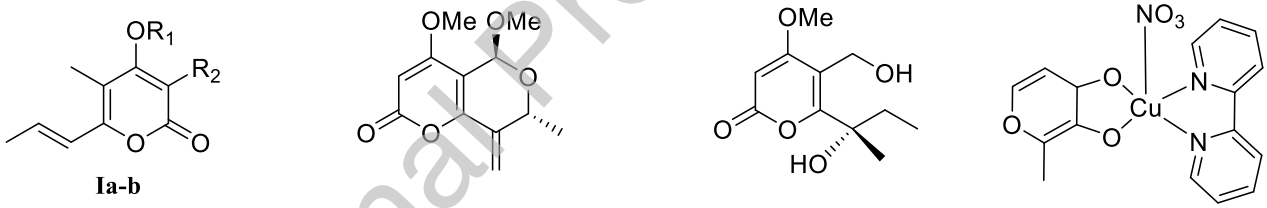

Ia-b

Udagawanones A and B

A. R_1 = Me; R_2 = -CH_2OH

B. R_1 = H; R_2 = -CHO

IIa

IIb

IIa Pleospyrones A; IC_{50}=1.26 mM (BGC-823)

IIb Pleospyrones D; IC_{50}=29.6 mM (NCI-HI650)

III

Cu(bpy)(maltol)(NO_3)

IC_{50}= 248 mg/mL

Figure 1: Structures of some bioactive compounds

Non-covalent interactions have extensive applications in different fields of science.[22] Since the physiological properties associated with a material greatly differ due to the presence of some peculiar non-covalent interactions. [23] The biological function associated with a bio-macromolecule can be qualitative explored in order to identify the existence of non-covalent interactions. [24–26] In addition, molecular recognition, being one of the fundamental biological step, is also governed largely by non-covalent interactions. Exploration of non-covalent interactions will help in fine-tuning the biological role associated with a molecule and opens new horizons for developing new generation of biologically significant molecules.[27] In continuation of our interest in the field of metal complex chemistry [28–30] we herein, explored the synthesis, non-covalent interactions, electrostatic properties and antibacterial potential of copper

complexes of carbohydrazide of pyrone (DHA) through solvent binding/complexation. The study was aimed at exploring the biological potential of newly synthesized solvent coordinated copper complexes and their comparison with the initially formed copper complex.

2 Experimental

2.1 General methods and materials

Dehydroacetic acid (DHA) and ethyl benzoate were purchased from Sigma Aldrich and used without further purification. Methanol and *N*,*N*-dimethylformamide were obtained from Fischer Scientific Pvt. Ltd. Isopropylamine, ethylene diamine, ethanol amine, *di*-isobutylamine, dimethylamine and anhydrous copper acetate were purchased from Avra chemicals and used as supplied.

2.2 Instrumentation

Elemental analysis was performed on FLASH EA 1112 Series CHNS Analyzer. The FTIR spectra were recorded on Perkin-Elmer FTIR 2000 spectrometer. The thermal gravimetric analysis (TGA) was carried out on SDT Q600 (V20.9 Build 20) instrument (Artisan Technology Group, Champaign, IL) under N_2 atmosphere. Single crystal X-ray diffraction data were collected using a Super-Nova diffractometer equipped with a micro-focus sealed tube. HRMS of all synthesized solvated complexes (5a-5g) was recorded on LC-MS Spectrometer Model Q-ToF (Figure 6S-12S, Table 15S). Antibacterial activity of the title compounds was carried out at IIIM-CSIR, Research Institute in Jammu, India.

2.3 Synthesis of ligand and complexes

2.3.1 Synthesis of benzohydrazide (1)

To a stirred solution of ethyl benzoate in ethanol, an ethanolic solution of hydrazine hydrate was added dropwise. The reaction mixture was then refluxed for 7-8 h and the precipitate thus formed was allowed to cool at room temperature and collected through filtration, washed thoroughly with cold ethanol to give pure benzohydrazide. Yield: 87%; melting point: 112-114°C (lit. mp [31]: 115 °C); IR ($\nu_{max,}$ cm^{-1}): 3353, 3325, 1643, 1590.

2.3.2 Synthesis of ligand DHB (3)

The benzohydrazide (**1**) formed was dissolved in a 50 mL round bottom flask using ethanol. To this an ethanolic solution of dehydroacetic acid (**2**) was added and the resulting reaction mixture was refluxed for 3 h at 80 °C and then stirred for 24 h at room temperature. The yellow solid thus obtained was filtered and recrystallized from hot ethanol. The precipitate thus formed was filtered under vacuum, washed with cold ethanol, and dried in vacuum as per the literature reported method. [32] Yield 91%; IR($\nu_{max,}$ cm^{-1}): 3153

(NH),1639 (C=N); Elemental analysis calculated for $C_{15}H_{14}N_2O_4$: C, 62.93; H, 4.93; N, 9.79. Found C, 62.85; H, 4.98; N, 9.84.

2.3.3 Synthesis of metal complex 4

To an ethanolic solution of (*E*)-*N*-(1-(2-hydroxy-6-methyl-4-oxo-4*H*-pyran-3-yl)benzohydrazide (**3**) a hot ethanolic solution of $[Cu(OAc)_2].H_2O$ was added with constant stirring (metal-ligand ratio of 1:1). The reaction mixture was refluxed for 1 h and further stirred for 24 h at room temperature. The resulting green precipitates were filtered and then dried in an oven. The resulted precipitate in ethanolic solution kept at room temperature for evaporation, afforded rod shaped blue crystals after 2 days.

2.3.3.1 Synthesis of solvated metal complex 5a

Ethanolamine was added dropwise to a hot methanolic solution of copper complex **(4)**. Clear solution of the reaction mixture was obtained after heating at 60°C. The solution was kept at slow evaporation at room temperature, and needle shaped crystals were obtained after one week. Yield 60%; IR ($\nu_{max,}$ cm^{-1}): 3372, 3280, 2941, 1674, 1639, 1557, 1515, 1442, 1348, 1255; Elemental analysis calculated for $C_{17}H_{19}CuN_3O_5$: C, 49.94; H, 4.68; N, 10.28. Found C, 49.90; H, 4.62; N, 10.23; HRMS (m/z): Calcd:408 Found:409.06$[M+H]^+$

2.3.3.2 Synthesis of solvated metal complex 5b

A clear solution was formed when methanol (20 mL) was added dropwise to the conical flask containing copper complex **(4)**. The content of the flask was heated gently at 60°C. Block shape crystals suitable for single-crystal X-ray diffraction were obtained by evaporating the solution at room temperature for five days. Yield 70%; IR ($\nu_{max,}$ cm^{-1}): 3542, 3399, 3056, 1671, 1615, 1585, 1557, 1445, 1350, 1239; Elemental analysis calculated for $C_{16}H_{16}CuN_2O_5$: C, 50.59; H, 4.25; N, 7.37. Found C, 50.51; H, 4.15; N, 7.29; HRMS (m/z): Calcd: 379 Found: 380.04 $[M+H]^+$

2.3.3.3 Synthesis of solvated metal complex 5c

DMF was added dropwise to a hot methanolic solution of copper complex **(4)** till the solution became clear and then gently warm the mixture at 60°C. Needle shaped crystals suitable for single crystal X-ray diffraction were obtained on slow evaporation for 10-11 days. Yield 58%; IR($\nu_{max,}$ cm^{-1}): 3546, 3403, 3051, 1671, 1617, 1557, 1523, 1445, 1351, 1239; Elemental analysis calculated for$C_{18}H_{19}CuN_3O_5$: C, 51.36; H, 4.55; N, 9.98. Found C, 51.31; H, 4.52; N, 9.94; HRMS (m/z): Calcd: 420 Found: 421.53 $[M+H]^+$

2.3.3.4 Synthesis of solvated metal complex 5d

To the hot methanolic solution (10 mL) of copper complex **(4)**, dimethyl amine was added dropwise till the solution becomes and heat the solution at 60°C. Needle shaped crystals were obtained on slow evaporation of the solvent at room temperature after 20 days. Yield 65%; Elemental analysis calculated for $C_{17}H_{19}CuN_3O_4$:

C, 51.97; H, 4.87; N, 10.70; Found C, 51.91; H, 4.80; N, 10.66; HRMS (m/z): Calcd: 392 Found: 393.08 $[M+H]^+$

2.3.3.5 Synthesis of solvated metal complex 5e

To a conical flask containing 10 mL of methanolic solution of copper complex **(4)**, isopropyl amine was added dropwise till the solution becomes clear and heated the solution at 60°C. Needle shape crystals suitable for single-crystal X-ray diffraction were obtained by evaporating the solution at room temperature for two weeks. Yield 76%; IR ($\nu_{max,}$ cm^{-1}): 3325, 3272, 2978, 1679, 1645, 1562, 1515, 1444, 1351, 1189; Elemental analysis calculated for $C_{18}H_{21}CuN_3O_4$: C, 53.13; H, 5.20; N, 10.33; Found C, 53.06; H, 5.15; N, 10.30; HRMS (m/z): Calcd: 406 Found:407.09 $[M+H]^+$

2.3.3.6 Synthesis of solvated metal complex 5f

To a hot methanolic solution (10 mL) of copper complex **(4)**, *di*-isobutylamine was added dropwise till the solution become clear and heated the solution at 60°C. The solution was kept for slow evaporation at room temperature. Needle shaped crystals were obtained after two weeks. IR ($\nu_{max,}$ cm^{-1}): 3348, 2958, 1684, 1662, 1557, 1518, 1445, 1347, 1230; Elemental analysis calculated for $C_{23}H_{31}CuN_3O_4$: C, 57.91; H, 6.55; N, 8.81. Found C, 57.87; H, 6.50; N, 8.78; HRMS (m/z): Calcd: 476 Found: 477.16 $[M+H]^+$

2.3.3.7 Synthesis of solvated metal complex 5g

Ethylene diamine was dropwise added to the hot methanolic solution of the copper complex **(4)** till it became clear and heated the solution at 60°C. The solution was allowed to kept at slow evaporation at room temperature. Needle shaped crystals suitable for single crystal X-ray diffraction was obtained after two weeks. IR ($\nu_{max,}$ cm^{-1}): 3390, 3248, 3158, 2864, 1683, 1561, 1513, 1444, 1348, 1168; Elemental analysis calculated for $C_{17}H_{20}CuN_4O_4$: C, 50.06; H, 4.94; N, 13.74. Found C, 50.02; H, 4.90; N, 13.69; HRMS (m/z): Calcd: 407 Found: 407.96 $[M+H]^+$

2.4 Antimicrobial activity

The compounds **(3,4 and 5)** were evaluated for their antibacterial and antifungal activity against four bacterial lines, Gram-positive *Staphylococcus aureus* ATCC 25923, *Bacillus subtilis* ATCC 6633, and Gram-negative *Escherichia coli* ATCC 25922, *Pseudomonas aeruginosa* ATCC 27853) and two fungal strains (*Aspergillus niger* ATCC 16404, *Candida albicans* ATCC 24433). The antibacterial and antifungal assays were performed in accordance with the procedures outlined by Clinical and Standards Institute (CLSI) [33–35]. Mueller-Hinton Agar (MHA) and Mueller-Hinton Broth (MHB) was prepared as per the manufacturer's instructions (HiMedia Laboratories, India). The pre-cultures of the bacterial strains were prepared in MHB by fresh inoculums of the cultures incubated at 37°C for 18-24 h, at 100 rpm shaking, to obtain concentrations of approximately 5 to 6 log CFU/mL (evaluated and adjusted photometrically at 625 nm). The

bacterial suspensions were further diluted with MHB to obtain a final inoculum of 5×10^5 CFU/mL. The assays were performed in clear 96 well microtiter plates. The compounds were dissolved in DMSO to make a stock solution of 10 mM. Initially the compounds were screened for antibacterial/antifungal activity at slight higher concentration (128 µM), and those showing inhibition in primary screening were further tested at different concentrations to obtain MIC and MBC values (Table 2). Each experiment was accompanied by a positive control containing broth, pathogen and a known inhibitory compound (Ciprofloxacin); a negative control containing broth and pathogen. Amphotericin B was used as positive control during antifungal screening of compounds. The plates were incubated for 24 h at 37°C with agitation and then observations were recorded visually. The minimum concentration of the compound at which there is no visual growth was observed is considered as MIC. A loopful inoculum from the wells containing no visual growth was streaked on the Tryptic Soya Agar media and incubated for 24 h at 37°C to record MBC. In case of fungi, the test was done in Saubroud Dextrose Broth (SDB) for MIC and Saubroud Dextrose Agar (SDA) for MFC and plates were kept for 48 h (instead of 24 h as for bacteria). All the experiments were performed in triplicate and the results were described as their mean.

2.5 X-ray crystallographic analyses

All the crystals were mounted on Hampton cryoloops. Geometric and intensity data for all the crystals were collected at room temperature using a Rigaku Super-Nova diffractometer equipped with a micro-focus sealed X-ray tube with Mo-Kα radiation (λ=0.71073 Å), and CCD HyPix3000 detector. The CrysAlisPro software [36] was used for data acquisition and reduction. The absorptions were corrected by SCALE3 ABSPACK multi-scan method. Using Olex2 package [37], all the structures were solved with direct methods [38] and refined by the full-matrix least-squares methods based on F^2 implemented in ShelXL. [39] The structural analysis of complexes **5b**, **5c** and **5g** shows the presence of a lattice methanol molecule. Hydrogen atoms were fixed at geometrical calculated positions except those of alcohol molecules in complex **5b**, which were detected on the difference Fourier map. All the non-hydrogen atoms were refined with anisotropic thermal parameters. Crystallographic data and details of structural refinements, bond lengths, angles and hydrogen bond geometric parameters of all complex are summarized in Table S1-S7.

Crystallographic data have been deposited with the Cambridge Crystallographic Data Centre as supplementary publication no. CCDC-1948211 for complex **4**, 1992007, 1992010-13, 1992017, and 1992020 for complexes **5d**, **5e**, **5a**, **5c**, **5f**, **5b** and **5g**, respectively. Copies of the data can be obtained free of charge on application to The Director, CCDC, 12 Union Road, Cambridge CB21EZ, UK (fax: Int. code +(1223)336-033; e-mail: deposit@ccdc.cam.ac.uk).

2.6 Computational Details

The single point energy calculations were done for all the metal complexes by using Gaussian 09 program and the coordinates from crystallographic analyses. DFT based method Becke's three parameter hybrid functional (B3) for the exchange part and the Lee-Yang-Parr (LYP)[40] correlation function at 6-311+G(d) level was used all C, H, N and O atoms, while LANL2DZ basis set was used for Cu metal.[41] The visualization of optimized geometry was performed using Avogadro 1.2 package. Crystal explorer program was used for Hirshfeld surfaces analysis and generating fingerprint plots.

3 Results and Discussion

3.1 Synthesis and characterization

The carbohydrazide ligand (*Z*)-*N*-((*E*)-1-(4-hydroxy-6-methyl-2-oxo-2*H*-pyran-3-yl)ethylidene) benzohydrazonic acid (**3**) was synthesized by the reaction of DHA (**2**) and benzohydrazide (**1**) in refluxing methanol. The benzohydrazide was firstly synthesized from the condensation of ethyl benzoate with hydrazine hydrate in refluxing ethanol. Ligand **3**, thus formed was reacted with copper acetate in the presence of ethanol to afford the trigonal bipyramidal copper complex **4**, showing coordination with two molecules of ligand and one molecule of water, and their detail structural description reported earlier by our group. [28] Moreover, the related crystallographic parameters are listed in Tables 1S-2S and X-ray structure is shown in Figure 1S. Then complex **4** was reacted with equimolar amount of ethanolamine, and it was observed that the new incoming nucleophilic solvent (characterized by X-ray structural analysis, Figure 2) replaced the monodentate ligand molecule and aqua species. The structure of all the metal complex alongwith their synthetic route is shown in Scheme 1.

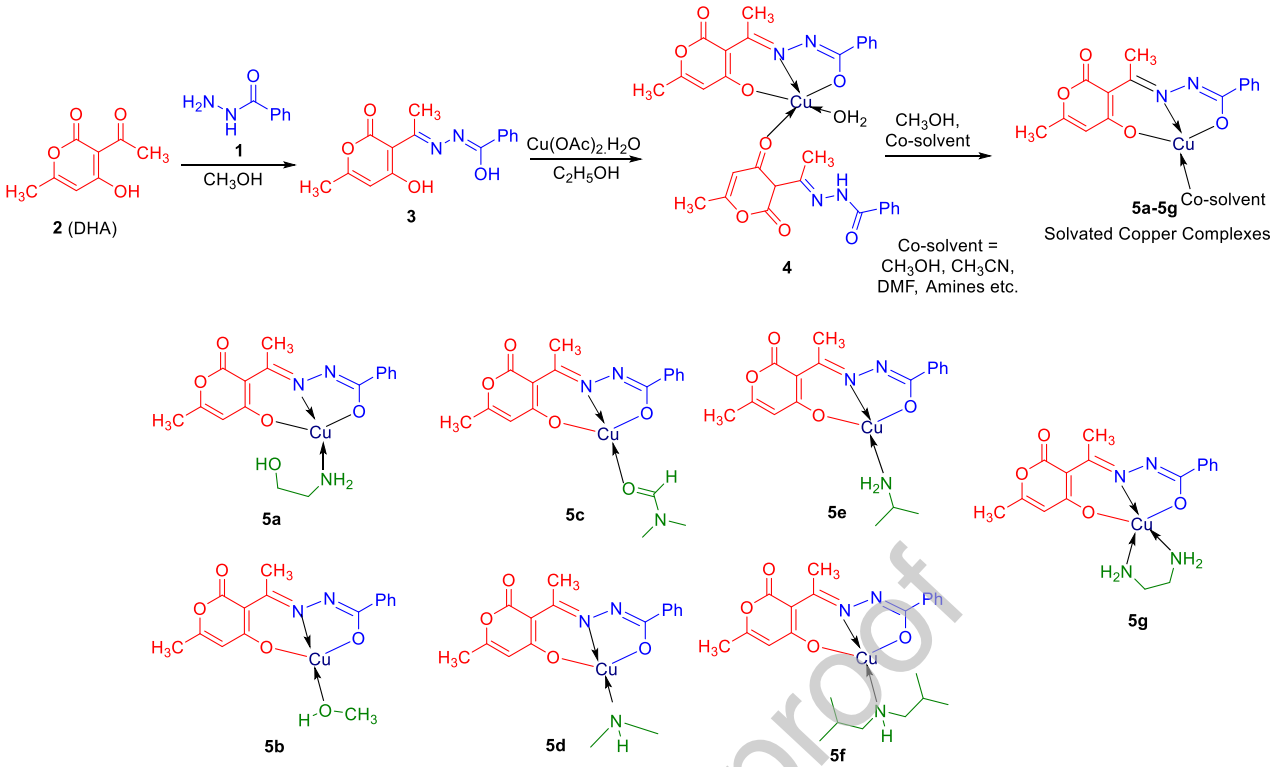

Scheme 1: Synthetic outline for the synthesis of solvated complexes **5a-5g**

Possibly the mono-coordinated carbohydrazide ligand was a labile leaving group which was easily replaced by the incoming nucleophilic solvent. Then, to generalize the concept of solvation of complex with co-solvent, an attempt was made to explore the reaction with various amines and other nucleophiles such as isopropylamine, *di*-isobutylamine, ethylenediamine, dimethylformamide, and dimethylamine. The structure of all the synthesized complexes (**5a-5g)** was confirmed by single crystal X-ray diffraction analysis.

3.1.1 Description of crystal structures

All the complexes have been synthesized with copper (II) salt, doubly deprotonated tridentate ligand H_2L (H_2L = *N'*-(1-(2-hydroxy-6-methyl-4-oxo-4*H*-pyran-3-yl)ethylidene)benzohydrazide and various amines, methanol or dimethylformamide and characterized by single crystal diffraction analysis. At our knowledge, none of the reported copper complexes with this ligand using different solvent have been structurally reported.

3.1.1.1 Complexes $[Cu(L)(NH_2CH_2CH_2OH)]$ (5a), $[Cu(L)(NH(CH_3)_2)]$ (5d), and $[Cu(L)(NH(CH_2CH(CH_3)_2)_2]$ (5f)

The X-ray structural analysis shows that the complex **5a** crystallizes in monoclinic system with space group *C*2/c, while **5d** and **5f** crystallize in triclinic of *P*-1 space group. In the complexes **5a**, **5d** and **5f** the copper (II) center exhibits a square planar coordination geometry, realized by the tridentate ligand through the imino

N, the deprotonated OH of pyranone ring and the amide carboxyl oxygen donors, and by a neutral molecule bound with the primary (in **5a**) or secondary amine (**5d**, **5f**) nitrogen donor (Figure 2).

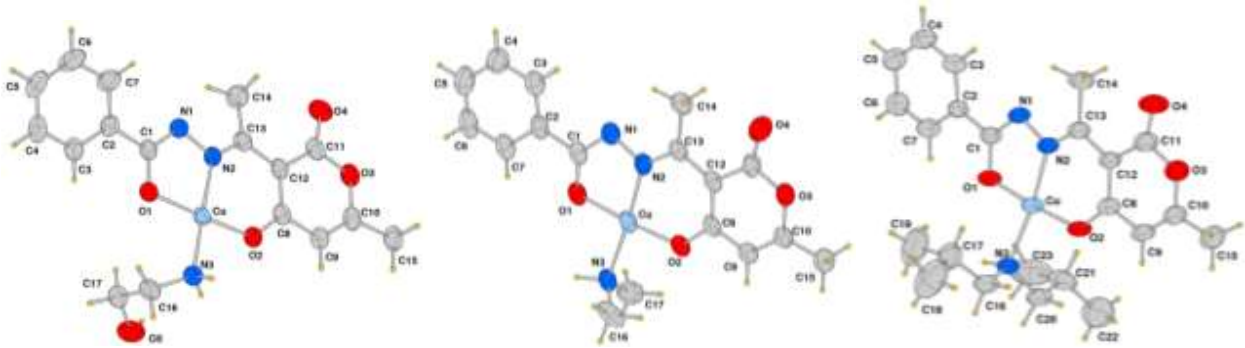

Figure 2: Molecular structure of the complexes **5a**, **5d** and **5f** (ORTEP diagram with 50% probability thermal ellipsoids, 35% for **5f**)

The Cu-O bond distances vary from 1.868(2) to 1.907(3) Å, with about 0.02 Å shorter for the lactone oxoanion O2 and the Cu-N(imino) ones vary from to 1.913(3) to 1.9265(16) Å. On the other side, the Cu-N(amine) bond lengths appear slightly shorter in **5a**, of 1.9882(16) Å, with respect to the values measured in **5d** and **5f** (2.012(2) and 2.008(3) Å), thus steric effects are prevailing over basicity. The coordination bond distances reported in Table 4S are indicative of the deviations from ideal values and the O1-Cu-N2 angle in the five membered ring shows the narrow value of ca. 83°.

In the crystal packing of **5a** the complexes are arranged in pair about a center of symmetry where the ethanolamine alcoholic group of each complex forms a hydrogen bond with oxygen O4 of the symmetry related species (O5…O4 = 2.773(3) Å). In addition, these dimers are weakly connected through N3-H…O5'' hydrogen bond (N3…O5'' = 3.066(3) Å) to give rise to a polymeric arrangement (Figure 3). Complexes **5d** are also connected to form a polymeric arrangement realized by weak N3-H…O4' hydrogen bonds (Figure 4, N3…O4' = 3.166(4) Å). Conventional hydrogen bond parameters for all structures reported are listed in Table 7S.

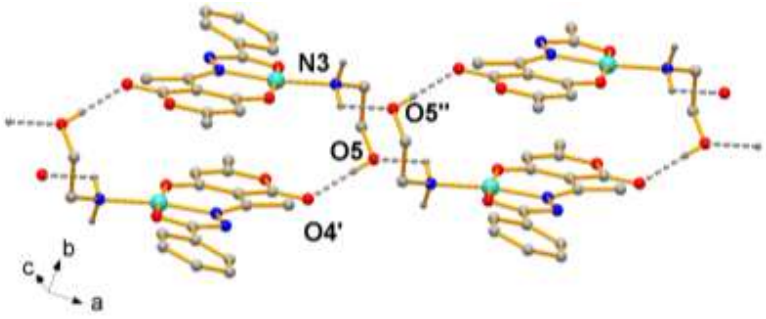

Figure 3: Complexes **5a** arranged about a crystallographic symmetry center connected by O5-H…O4' hydrogen bonds and further by N3-H…O5'' interactions to form a polymeric arrangement.

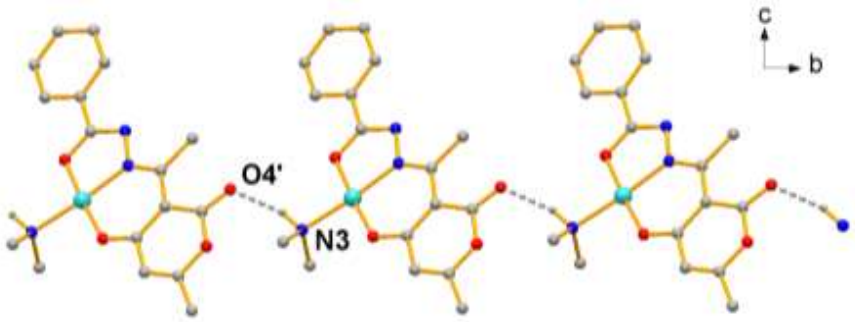

Figure 4: Crystal packing of complexes **5d** connected by weak N3-H…O4' hydrogen bonds to form a polymeric chain

3.1.1.2 Complexes [Cu(L)(CH_3OH)]·(CH_3OH) (5b), [Cu(L)(dmf)](CH_3OH) (5c), and [Cu(L)($NH_2CH(CH_3)_2$)] (5e)

Complexes **5b** and **5c** crystallize in triclinic system of *P-1*space group, both with a lattice methanol molecule, while complex **5e** crystallizes in monoclinic system with $P2_1/c$ space group. The coordination geometry of copper ion in all cases is square pyramidal where the basal plane is occupied by the *tris*-chelating ligand L through the ONO donor set and one methanol in **5b**, a dmf molecule in **5c**, an *i*Pr-amine in **5e**. Oxygen atom O4' (in **5b** and **5e**) and O1' (in **5c**), of a symmetry related molecule, resides at the apex of the pyramidal environment (Figure 5), so that in solid state the complexes are centrosymmetric dinuclear species (Figures 2S-4S of supplementary material).

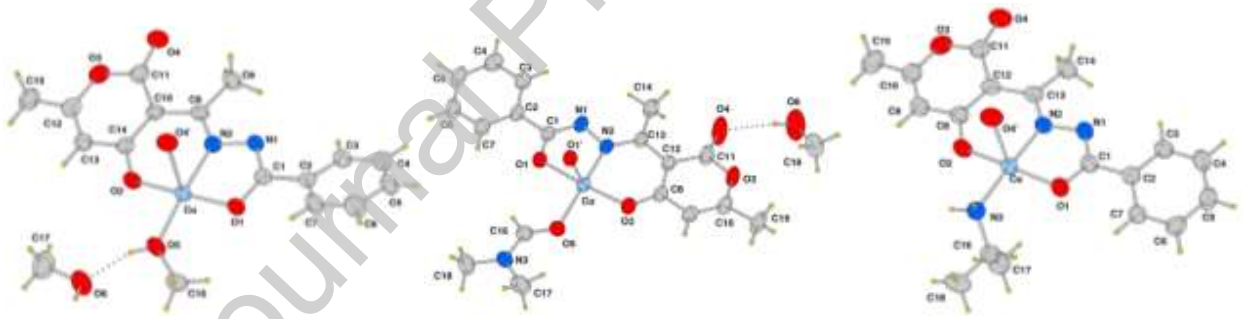

Figure 5: ORTEP diagram of complexes **5b**, **5c** and **5e** with thermal ellipsoids set at 50% probability level

The coordinated bond distances and angles are reported in Table 5S. The Cu-O and Cu-N bond lengths involving ligand L show comparable trend as that observed in complexes described above, while the Cu-OCH_3 and Cu-O(dmf) are of 1.943(3) and 1.9757(17) Å for **5b** and **5c**, respectively, which are likely affected by the H bond with a lattice methanol molecule. The Cu-N3 in **5e** is 1.992(2) Å, in accord with the value in **5a** (1.9882(16) Å) for a primary amine. The apical Cu-O distances are longer for Jahn-Teller effect, of 2.881(4), 2.6221(18), and 2.678(2) in **5b**, **5c** and **5e**, respectively. Although the former distance appears rather long, the interaction is apparent by O4 displacement of 0.23 Å from the lactone mean plane towards the copper atom of the symmetry related complex.

Complexes **5b** and **5c** crystallize with a lattice methanol molecule, a feature affecting the crystal packing of both. In **5b** the methanol molecule acts as acceptor from the alcoholic coordinated group and as donor towards oxygen O4' of a symmetry related molecule (O5…O6 = 2.616(5) Å; O6...O4' = 2.741(5) Å, Figure 6), thus connecting the complex dimers and forming a polymeric chain, elongated in the direction of axis *b*. On the other hand in crystal packing of **5c** the methanol molecule is H-bound to oxygen O4 as indicated in Figure 5 (O6…O4 = 2.803(4) Å).

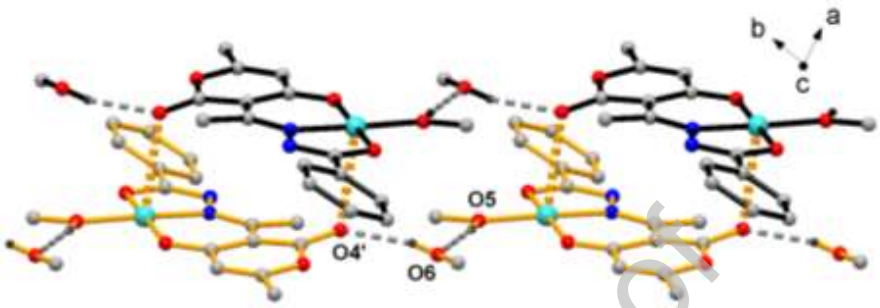

Figure 6: Polymeric chain built by H-bond in the crystal packing of **5b** with indication of the complex dimers connected by Cu-O4' bonds. (O4' at 1+x, -1+y, z; only H atoms involved in interactions are shown**)**

3.1.1.3 Complex [Cu(L)(en)](CH$_3$OH) (5g)

Complex **5g** crystallizes in triclinic system of space group *P*-1 with a lattice methanol molecule. Figure 7 depicts an Ortep view, while a selection of bond distances and angles are listed in Table 6S.

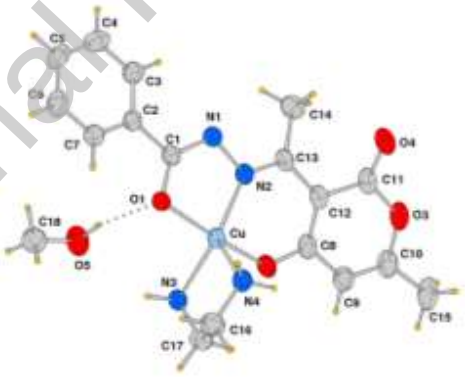

Figure 7: Molecular structure of complex**5g** (ORTEP diagram, with 50% probability thermal ellipsoids).

The metal centre is five coordinated in a highly distorted square pyramidal environment realized by the ONO donor set of tridentate ligand L and by a chelating ethylendiamine. The coordination geometry is confirmed by the trigonality τ index of 0.03 (being = 0 or 1 for a perfect square pyramidal and trigonal bipyramidal geometry, respectively).[42] The Cu–O1, Cu–O2 and Cu-N2 bond distances of chelating ligand (1.9505(13), 1.9126(14) and 1.9335(17) Å, respectively) follow a trend similar to previous complexes, but all appear slightly longer. The Cu-N(en) bond lengths of ethylenamine are of 2.0357(17) and 2.2969(17) Å, significantly different as expected for a square pyramidal copper (II) complex. The bond angles N2-Cu-N4

and N(3) Cu-N(4), of 114.51(6) and 81.62(6)°, are indicative of deviation from an ideal apical position of N4 in the square pyramidal geometry.

The lattice methanol molecule and amine groups generate a one-dimensional hydrogen bonding scheme forming a polymer developed in the [101] crystallographic direction. The O5…O1 distance is 2.776(2) Å, while the N-O interactions are weaker, of about 3.0 Å (Figure 8).

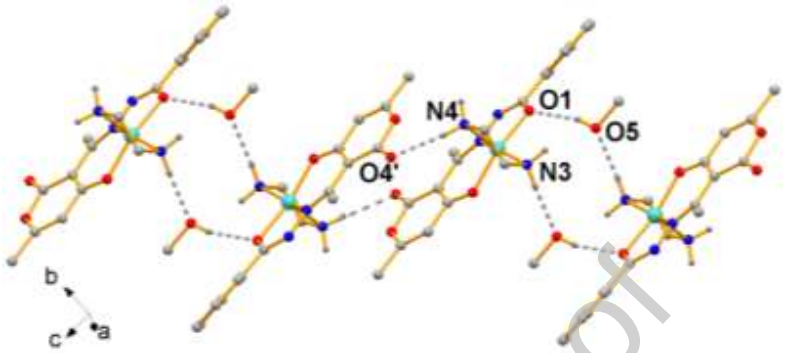

Figure 8: 1D polymeric arrangement of complexes **5g** connected by H-bonds involving the bridging methanol and amine N3/N4 groups.

The crystal structures of all the complexes do not show any significant π-π interaction among phenyl rings, and the packing is mainly dominated by H-bonds as described. The coordinated bond distances and angles of complexes reported are in good agreement with values measured in the two copper complexes comprising an analogous ligand [43,44].

3.1.2 Hirshfeld surface analysis

In a crystal structure, hydrogen bond donors and acceptors result into intermolecular interactions of variable range that are responsible for molecular assembly in solid state. These interactions can be explored in a quantitative manner using Hirshfeld Surface (HS) analysis.[45] In addition to short contacts, the surface characteristic of molecular systems can also be visualized using HS analysis. The presence of solvent in the crystal structure effect various intramolecular interactions operative in case of compound. HS were used to investigate the solvates and voids. In some cases, solvents have a stabilizing effect on the crystal structure of the compounds. On the other hand, the various intramolecular interactions are also effected by the presence of a solvent molecule. The total percentage contribution of interaction is larger in the presence of a solvent that represent the presence of disorder. Cruz Cabeza *et al.* have demonstrated the role of solvents in stabilizing crystal structures by computational methods.[46] The phenomenon of formation of isomorphic desolvates of organic compounds is well-documented in the literature. For example, hydrates that desolvate yet retain their original crystal lattice, which is less stable than its solvated form, are known for cephalexin, cefaclor, erythromycin A and spirapril hydrochloride hydrates, to name but a few.[47]

Void refers to isolated cavity filled with solvent or guest molecule and resulted into permanent channels by their linking in different dimensions. This feature is associated with the porosity of crystals and used for the transportation of small molecules. The mapping of the procrystal isosurface within a unit cell has been implemented in Crystal Explorer, volumes within the voids defined in this manner, and their surface areas, are computed trivially and routinely. The exact isovalues of the procrystal electron density provide physically meaningful volumes and surface areas of voids in molecular crystals. HS are mapped using color-coded surfaces with red, blue, and white color. The intermolecular contacts are visualized using d_{norm} value, where intermolecular contacts shorter than vdW are associated with a negative d_{norm} value and represented by red color, larger with positive d_{norm} by blue color, while contacts equal to vdW distance are shown by white color and associated to zero d_{norm} value. The related π-π interactions among aromatic regions are obtained along a specific axis by shape index with blue, red, and white colored zones. The curvedness provides information about the curvature of the surface, where low and large values are associated to flat surface and sharp curvature, respectively. The larger flat regions have a boundary of blue color. The Hirshfeld surface for **5a** are over d_i (0.720 to 2.599 Å), d_e (0.720 to 2.488 Å), d_{norm} (-0.632 to 1.387 Å), shape index (-0.994 to 0.997 Å) and curvedness (-3.711 to 0.526 Å). The voids present on the surface have volume 419.40 Å^3 with area of 393.95 Å^2. The Hirshfeld surface for **5d** are over d_i (0.922 to 2.836 Å), d_e (0.923 to 2.544 Å), d_{norm} (-0.325 to 1.484 Å), shape index (-0.998 to 0.995 Å) and curvedness (-3.350 to 0.457 Å). The voids present on the surface have volume 414.10 Å^3 with area of 385.63 Å^2. For compound **5f,** HS are over d_i (1.037 to 2.609 Å), d_e (1.037 to 2.501 Å), d_{norm} (-0.097 to 1.479 Å), shape index (-0.998 to 0.995 Å) and curvedness (-4.477 to 0.748 Å). The voids present on the surface have volume 583.33 Å^3 with area of 488.62 Å^2 (Figure 9).

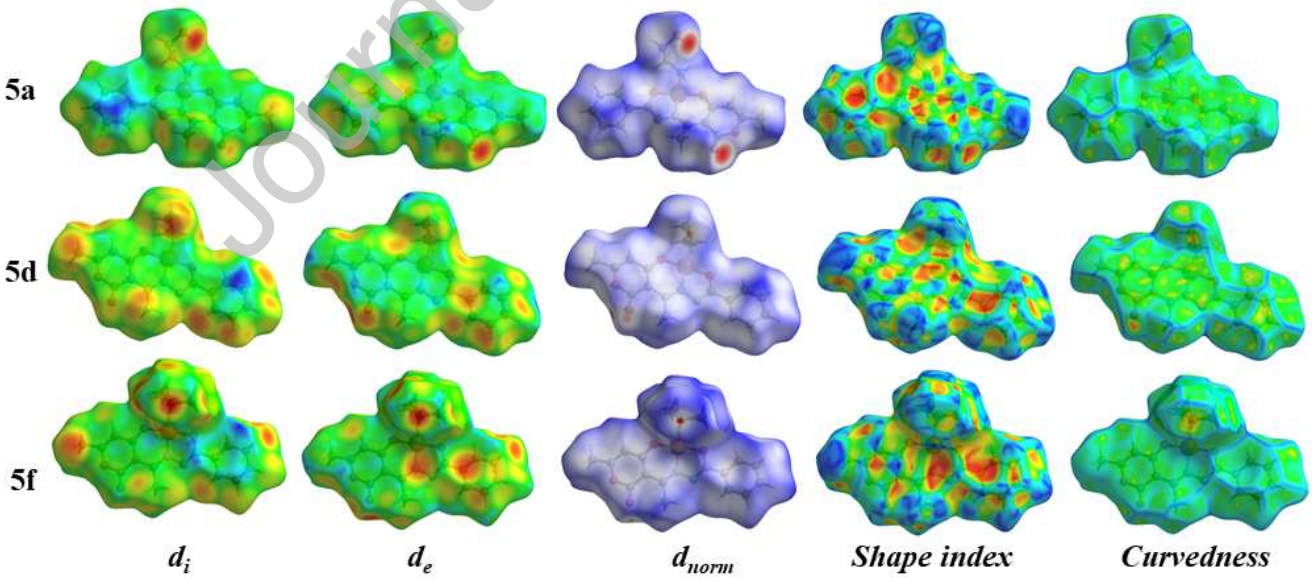

Figure 9: Hirshfeld surface analysis of **5a**, **5d** and **5f**

The Hirshfeld surface decomposed into 2D fingerprint to quantify the intra and intermolecular interactions present in case of **5a**, **5d** and **5f**. It was observed that in all the three cases the major contribution was from H-H interaction that makes 53.1%, 52.3% and 58.2% of the total contribution made by different interactions in **5b**, **5c** and **5e**, respectively. The contribution of O-H interaction in case of **5b**, **5c** and **5e** is 22.0%, 18.3% and 15.7% respectively. The other minor contributions are shown in Figure 10.

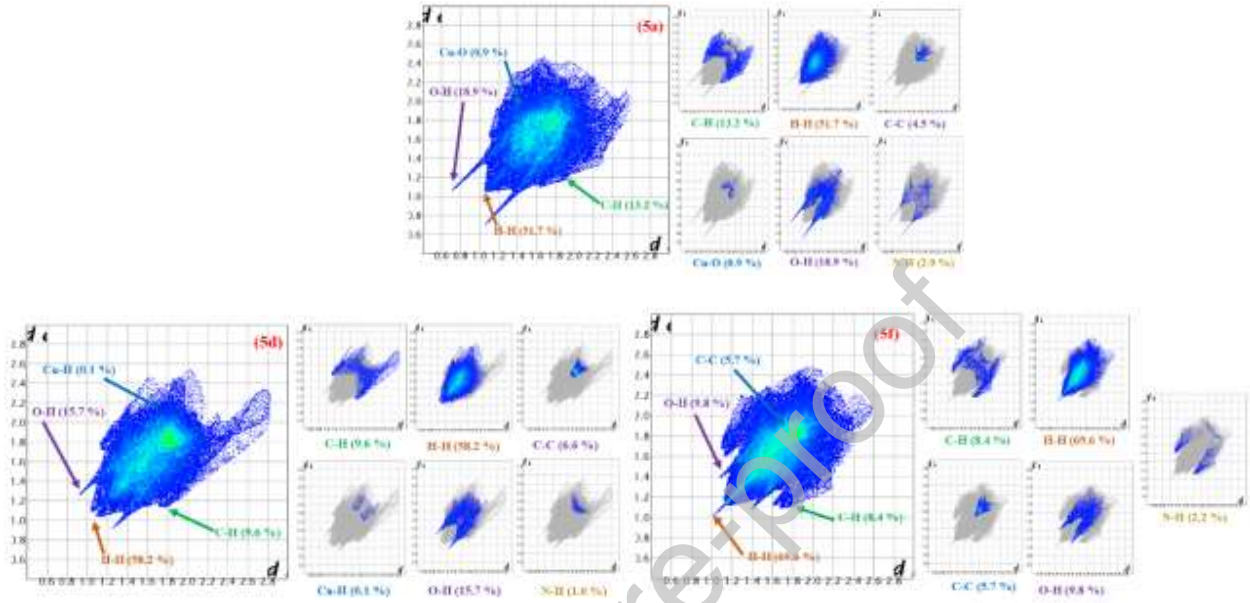

Figure 10: 2D fingerprint plot for **5a, 5d** and **5f**

The Hirshfeld surface for **5b** are over d_i (0.743 to 2.651 Å), d_e (0.743 to 2.507 Å), d_{norm} (-0.599 to 1.314 Å), shape index (-0.995 to 1.000 Å) and curvedness (-4.726 to 0.365 Å).The voids present on the surface have volume 428.00 Å^3 with area of 401.67 Å^2. The Hirshfeld surface for **5c** are over d_i (0.751 to 2.693 Å), d_e (0.753 to 2.601 Å), d_{norm} (-0.583 to 1.283 Å), shape index (-0.997 to 0.996 Å) and curvedness (-3.749 to 0.376 Å).The voids present on the surface have volume 492.50 Å^3 with area of 457.59 Å^2. For compound **5e** HS are over d_i (0.995 to 2.547 Å), d_e (0.994 to 2.499 Å), d_{norm} (-0.208 to 1.295 Å), shape index (-0.999 to 0.999 Å) and curvedness (-3.462 to 0.466 Å).The voids present on the surface have volume 449.70 Å^3 with area of 409.32 Å^2 (Figure 11).

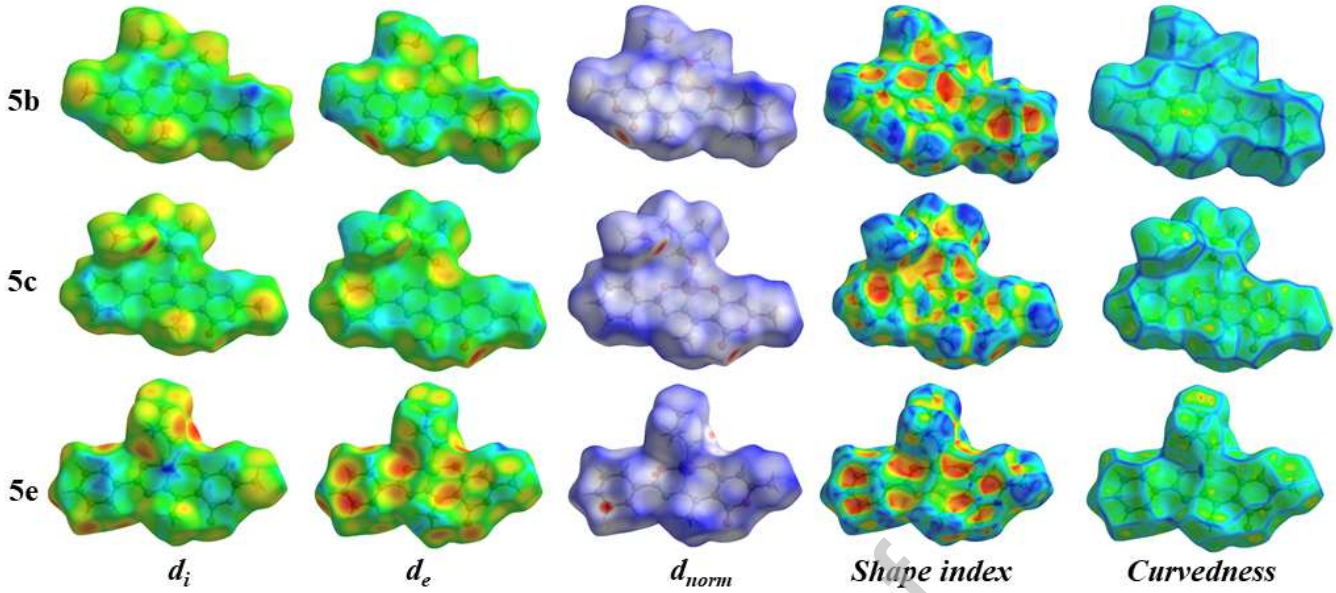

Figure 11: Hirshfeld surface analysis of **5b, 5c** and **5e**

The Hirshfeld surface decomposed into 2D fingerprint to quantify the intra and intermolecular interactions present in case of **5b**, **5c** and **5e**. It has been observed that in all the three cases the major contribution was from H-H interaction, which makes 69.6%, 51.7% and 55.7% of the total contribution made by different interactions in **5b**, **5c** and **5e**, respectively. The contribution of O-H interaction in case of **5b**, **5c** and **5e** is 9.8%, 18.9% and 18.3% respectively. The other minor contributions are shown in Figure 12.

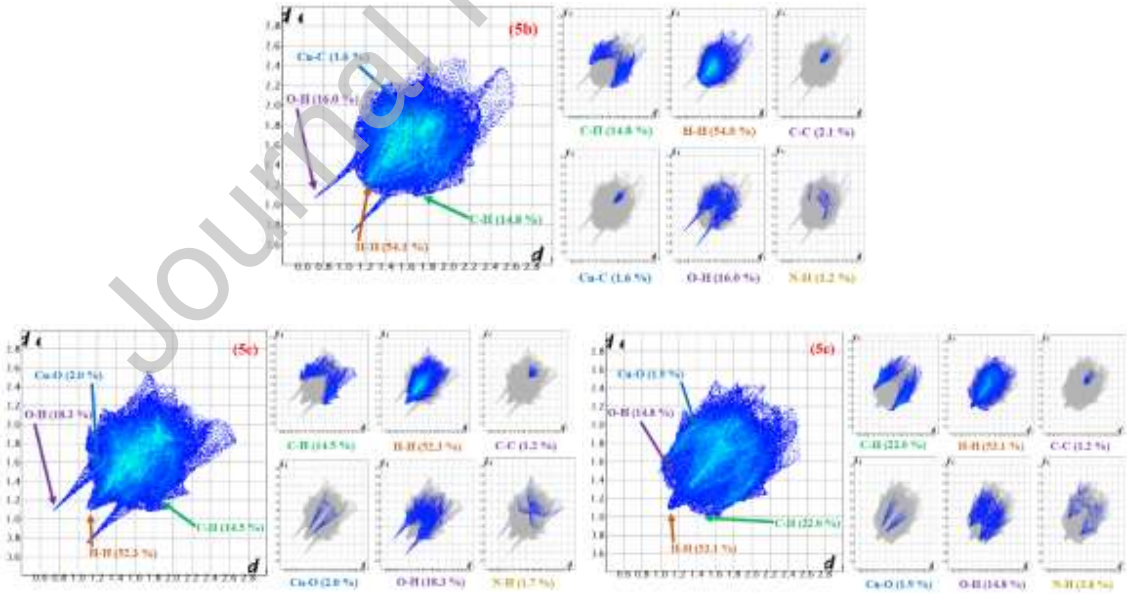

Figure 12: 2D fingerprint plot for **5b, 5c** and **5e**

Finally, the Hirshfeld surface for **5g** are over d_i (0.854 to 2.544 Å), d_e (0.854 to 2.590 Å), d_{norm} (-0.431 to 1.738 Å), shape index (-0.999 to 0.998 Å) and curvedness (-3.944 to 0.315 Å). The voids present on the surface have volume 482.09 Å^3 with area of 424.68 Å^2 (Figure 13).

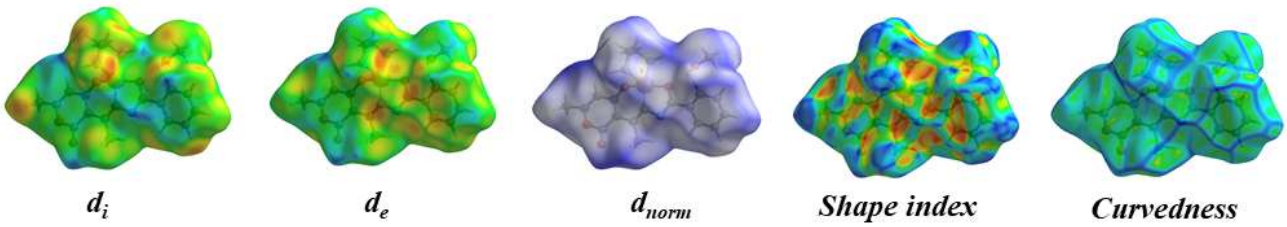

Figure 13: Hirshfeld surface analysis of **5g**

The HS was further decomposed into fingerprint region where H-H interactions contributes to a maximum of 54.0%. In addition to this, other significant contributions are from O-H and C-H contacts with overall contribution of 16.0% and 14.8%. The minor contribution of Cu-O, C-C, and N-H contact are recorded with 1.6%, 2.1%, and 1.2%, respectively (Figure 14).

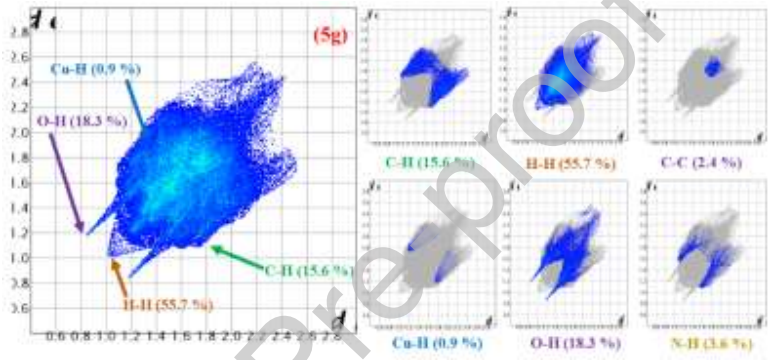

Figure 14: 2D fingerprint plot for **5g**

The supramolecular interactions discussed in crystallographic description are responsible for various polymeric forms in case of all the crystals. Hirshfeld surface analysis was done to explore atom based interactions present in case of all the complexes. It has been observed that the polymeric forms of all these crystals are mainly due to potential hydrogen bonding interaction. The higher percentage of O-H type interaction observed by the decomposition of Hirshfeld surface into 2D fingerprint region supports the formation of various polymeric arrangement due to potential O-H bonding in all the crystals. Moreover, various inter and intramolecular interactions present in case of all the metal complexes was calculated using PARST incorporated in Wingx. The self-assembly of all the metal complexes is primarily due to H-H and O-H type of interactions. The main D-H---A type interactions present in case of all the metal complexes has been listed in Table 8S-14S.

3.2 DFT studies

Frontier molecular orbitals HOMO and LUMO and their gap play a significant role in investigating the kinetic stability and chemical reactivity of a molecule.[48] The ability of a molecule to act as electron donor and acceptor solely depends upon the distribution of electrons and their energy in HOMO and LUMO.

Materials associated with large HOMO-LUMO gap have large kinetic stability, because it is difficult to add electrons into high energy lying LUMO orbitals.[49] Thus, compounds associated with large energy gap are associated with low chemical reactivity. Moreover, the electronic transitions associated with a molecule can also be explored using the time dependent approach. In order to investigate the electrostatic parameters associated with the present metal complexes **(5a-5g)**, single point energy was calculated for all of these in gas phase using by taking the atomic coordinates from crystallographic analyses. In order to formulate a relationship within electrostatic properties, all the metal complexes have been grouped similarly as done in crystal studies. In case of compound **5a**, the energy of HOMO and LUMO is -5.659 and -1.733 eV, respectively with an energy gap of 3.926 eV. The energy of frontier molecular orbitals for all other compounds has been summarized in Figure 15, which reveals that within 1st group, compound **5a** has high chemical stability with an energy difference of 3.926 eV in comparison with 3.845 and 3.895 eV for **5d** and **5f**, respectively. Similarly, in 2nd group compound **5c** is more stable with an energy difference of 3.976 eV in comparison with 3.221 and 3.923 eV for **5b** and **5e**, respectively. Among all seven metal complexes, compound **5c** shows the higher chemical stability based on HOMO-LUMO energy difference.

Koopman's theorem proposed several electrostatic parameters for molecular systems which can be assessed to determine the site selectivity and chemical reactivity of a molecule.[48] Various aspects of chemical reactivity associated with a molecule can be assessed directly by utilizing the information related with frontier molecular orbitals. Over the years, these reactivity indices have been utilized extensively for studying different facets of medicinal chemistry. Moreover, the dynamics of a reaction can also be studied by exploring the time dependent profile of these global descriptors. Chemical hardness (η), softness (s), chemical potential (μ), electronegativity (χ) and electrophilicity index (ω) are important global reactivity descriptors which could explain most of the physiochemical properties associated with a molecule.[49] Electrophilicity index (ω) is a definite and positive quantity that measures the stabilization energy when extra electronic charge is added to the system. Moreover, this descriptor also explains the transfer of charge in a chemical reaction, lower the value, lower will be the electrophilicity. The global reactivity descriptors calculated for all the metal complexes are listed in Table 1. The compound **5b** appears to be the most electrophilic, and compound **5g** the least among all complexes.

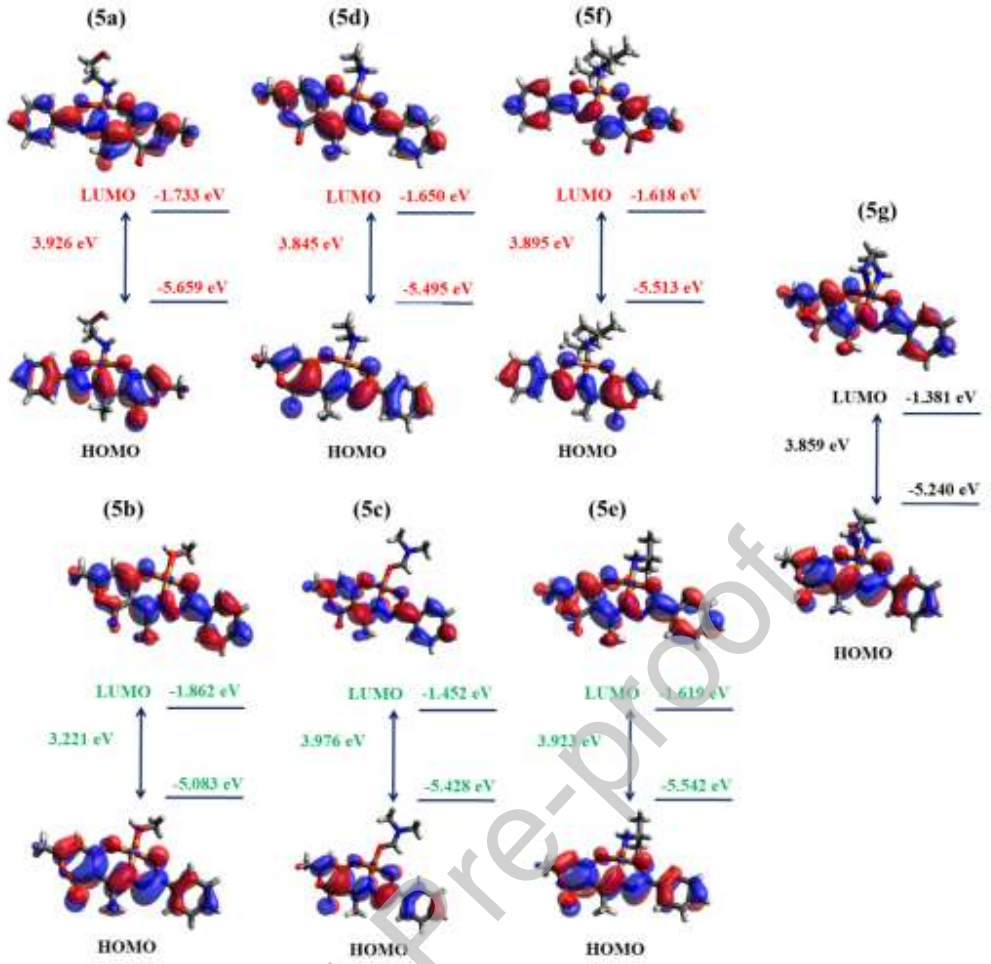

Figure 15: Frontier molecular orbitals for compounds **5a-5g**

Table 1: Electrostatic parameters for compounds **5a-5g** calculated in gas phase

Complex	HOMO	LUMO	Electronegativity χ = (I+A)/2	Chemical potential (μ)	Chemical hardness η= (I-A)/2	Chemical softness (s)	Electrophilicity Index (ω)
5a	-5.6590	-1.7330	3.6960	-3.6960	1.9630	0.2547	3.4795
5b	-5.0830	-1.8620	3.4725	-3.4725	1.6105	0.3105	3.7436
5c	-5.4280	-1.4520	3.4400	-3.4400	1.9880	0.2515	2.9763
5d	-5.4950	-1.6500	3.5725	-3.5725	1.9225	0.2601	3.3193
5e	-5.5420	-1.6190	3.5805	-3.5805	1.9615	0.2549	3.2679
5f	-5.5130	-1.6180	3.5655	-3.5655	1.9475	0.2567	3.2639
5g	-5.2400	-1.3810	3.3105	-3.3105	1.9295	0.2591	2.8400

3.3 TGA data

Thermogravimetric analysis is a useful technique to evaluate the stability of a complex. The synthesized solvated metal complexes undergone thermal decomposition over temperature range 25-1000°C under nitrogen atmosphere. The data strongly suggested that proposed formulas were correct for these complexes (Figure 5S). Thermogram of complex **5a** shows three degradation steps within the temperature range of 50-200, 200-445 and 445-950°C, which correspond to mass loss of 20.02, 50.60 and 18.20% respectively.

Thermogram of complex **5b** shows weight loss of 16.78, 35.62 and 31.14% in the temperature ranges 70-140, 300-440 and 440-920°C. While the TGA profile of complex **5c** shows a first decomposition stage between 70-140°C with weight loss of 15.57%, second occurred at 300-415°C with weight loss of 34.34% and third stage in between 415-920°C. The decomposition step for complex **5f** started in the temperature range 70-170°C with mass loss of 31.51%, then in range between 170-410°C with weight loss of 27.93% and third degradation stage between 410-915°C.

3.4 Antimicrobial activity

In the preliminary screening none of the synthesized complexes were found to have antifungal activity. Moreover, no antibacterial activity was observed against Gram-negative bacteria. The complex outer membrane (OM) in Gram-negative bacteria makes them tough to combat as compared to Gram-positive pathogens. The complex OM in Gram-negative bacteria acts as a selective barrier; they can modify their permeability properties, which have a major impact on the susceptibility to the antibiotics/molecules. [50] Synthesized complexes were found to be active against the Gram-positive Bacteria *Staphylococcus aureus* and *Bacillus subtilis*. All the compounds showed very good minimum inhibitory concentration and minimum bactericidal concentration against *B. subtilis*. Carbohydrazide ligand **3** didn't exhibited any type of activity against both the Gram-positive bacteria at the concentration 128 µM. On the basis of minimum inhibitory activity shown against bacteria, complex **4** and **5f** was found to be the most effective against *B. subtilis* with 32 µM MIC and MBC values. Compound **5f** also showed good MIC values against *S. aureus* (Table 2)**.** It is noteworthy that the Cu^{2+} was inactive at 128 µM concentration when tested for antimicrobial activity.

Table 2: MIC and MBC of compounds **5a**-**5g** against *S. aureus* and *B. subtilis*

	Staphylococcus aureus **(ATCC 25923)**			***Bacillus subtilis*** **(ATCC 6633)**		
Complex/Compound	**Primary screening at 128 µM**	**Minimum Inhibitory Concentration (MIC) µM**	**Minimum Bactericidal Concentration (MBC) µM**	**Primary screening at 128 µM**	**Minimum Inhibitory Concentration (MIC) µM**	**Minimum Bactericidal Concentration (MBC) µM**
3	NA	-	-	NA	-	-
4	+	64	64	+	32	32
5a	+	128	128	+	64	64
5b	+	128	128	+	64	64
5c	+	128	128	+	64	64
5d	+	128	128	+	64	64
5e	+	128	128	+	64	128
5f	+	64	128	+	32	32
5g	+	128	128	+	64	64

Ciprofloxacin	+	0.016	0.016	+	0.016	0.016

+ Samples shows antibacterial activity in primary screening; NA: Not active

4 Conclusion

In conclusion, an efficient and mild synthetic approach metal complexes of (*Z*)-*N*-((*E*)-1-(4-hydroxy-6-methyl-2-oxo-2*H*-pyran-3-yl)ethylidene)benzohydrazonic acid coordinated with solvated with various solvent molecules such as isopropylamine, di-isobutylamine, ethylenediamine, dimethylformamide, dimethylamine and methanol has been developed. The complexes were characterized extensively with the help of IR, TGA and single crystal X-ray analysis. The intermolecular interactions exist in case of all the complexes have been quantified using Hirshfeld surface analysis. The electrostatic properties associated with all these complexes was calculated using DFT studies. The synthesized copper complexes exhibited significant activity against the Gram-positive bacteria specifically against *B. subtilis*. Complex **4** and **5f** was found to be the most effective against *B. subtilis* with 32 μM MIC and MBC values. On the other hand, the complexes did not exhibit antifungal activity against the fungal strains *Candida albicans* and *Aspergillus niger*. Therefore, the synthesized metal complexes can act as selective antibacterial agents, since they exhibit activity only against Gram-positive bacteria.

Declaration of competing interest

The authors declare that they have no known competing financial interests or personal relationships that could have appeared to influence the work reported in this paper.

Acknowledgments

Authors thanks DST-FIST for single crystal facility, DST-PURSE and UGC-CAS for departmental support. Richa thanks CSIR for financial support in the form of JRF.

Credit author statement

Conceptualization	Ramesh Kataria, Ennio Zangrando, Jayant Sindhu, Vinod Kumar, SK Mehta
Methodology	Richa, Poonam Choudhary, Sundeep Jaglan, Rakesh Kumar
Software	SC Sahoo, Ramesh Kataria, Jayant Sindhu, Ennio Zangrando
Validation	Ramesh Kataria, Jayant Sindhu, Vinod Kumar, SK Mehta, SC Sahoo
Formal analysis	Richa, Rakesh, Jayant, Ramesh Kataria, Poonam Choudhary, Sundeep Jaglan
Investigation	Richa, Rakesh, Poonam Choudhary, Sundeep Jaglan
Resources	Ramesh Kataria, SK Mehta
Data Curation	Richa, SC Sahoo, Ramesh Kataria, Jayant Sindhu, Ennio Zangrando, Sunil Kumar
Writing Original Draft	Richa, Ramesh Kataria, Jayant Sindhu, Ennio Zangrando, Sunil Kumar, SK Mehta, Rakesh Kumar, Vinod Kumar
Writing Review & Editing	Richa, Ramesh Kataria, Jayant Sindhu, Ennio Zangrando, Sunil Kumar, SK Mehta, Rakesh Kumar, Vinod Kumar, Poonam Choudhary, Sundeep Jaglan, SC Sahoo
Visualization	Ramesh Kataria, SK. Mehta, Ennio Zangrando, Sunil Kumar, Vinod Kumar
Supervision	Ramesh Kataria
Project administration	Ramesh Kataria
Funding acquisition	Ramesh Kataria, SK Mehta

References:

[1] C.R. Culy, D. Clemett, L.R. Wiseman, Oxaliplatin: A review of its pharmacological properties and clinical efficacy in metastatic colorectal cancer and its potential in other malignancies, Drugs. 60 (2000) 895–924. https://doi.org/10.2165/00003495-200060040-00005.

[2] J.R. Eckardt, D.L. Bentsion, O.N. Lipatov, I.S. Polyakov, F.R. MacKintosh, D.A. Karlin, G.S. Baker, H.B. Breitz, Phase II study of picoplatin as second-line therapy for patients with small-cell lung cancer, J. Clin. Oncol. 27 (2009) 2046–2051. https://doi.org/10.1200/JCO.2008.19.3235.

[3] Y. Li, K. Zhou, Z. Wen, S. Cao, X. Shen, M. Lei, L. Gong, Copper(II)-Catalyzed Asymmetric Photoredox Reactions: Enantioselective Alkylation of Imines Driven by Visible Light, J. Am. Chem. Soc. 140 (2018) 15850–15858. https://doi.org/10.1021/jacs.8b09251.

[4] A.M. Suess, M.R. Uehling, W. Kaminsky, G. Lalic, Mechanism of Copper-Catalyzed Hydroalkylation of Alkynes: An Unexpected Role of Dinuclear Copper Complexes, J. Am. Chem. Soc. 137 (2015) 7747–7753. https://doi.org/10.1021/jacs.5b03086.

[5] Z. Ma, Q. Wang, E.C.B.A. Alegria, M.F.C.G. Da Silva, L.M.D.R.S. Martins, J.P. Telo, I. Correia, A.J.L. Pombeiro, Synthesis and structure of copper complexes of a N6O4 macrocyclic ligand and catalytic application in alcohol oxidation, Catalysts. 9 (2019). https://doi.org/10.3390/catal9050424.

[6] Z. Ma, A. V. Gurbanov, A.M. Maharramov, F.I. Guseinov, M.N. Kopylovich, F.I. Zubkov, K.T. Mahmudov, A.J.L. Pombeiro, Copper(II) arylhydrazone complexes as catalysts for C[sbnd]H activation in the Henry reaction in water, J. Mol. Catal. A Chem. 426 (2017) 526–533. https://doi.org/10.1016/j.molcata.2016.05.030.

[7] R.R. Zhuang, F.F. Jian, K. Wang, An electrochemical sensing platform based on a new copper complex for the determination of hydrogen peroxide and nitrite, Sci. Technol. Adv. Mater. 10 (2009). https://doi.org/10.1088/1468-6996/10/4/045001.

[8] M.G. Caglayan, S. Sheykhi, L. Mosca, P. Anzenbacher, Fluorescent zinc and copper complexes for detection of adrafinil in paper-based microfluidic devices, Chem. Commun. 52 (2016) 8279–8282. https://doi.org/10.1039/c6cc03640f.

[9] S.G. Leonardi, M. Bonyani, K. Ghosh, A.K. Dhara, L. Lombardo, N. Donato, G. Neri, Development of a novel Cu(II) complex modified electrode and a portable electrochemical analyzer for the determination of dissolved oxygen (DO) in water, Chemosensors. 4 (2016). https://doi.org/10.3390/chemosensors4020007.

[10] E.K. Efthimiadou, H. Thomadaki, Y. Sanakis, C.P. Raptopoulou, N. Katsaros, A. Scorilas, A. Karaliota, G. Psomas, Structure and biological properties of the copper(II) complex with the quinolone antibacterial drug N-propyl-norfloxacin and 2,2′-bipyridine, J. Inorg. Biochem. 101 (2007) 64–73. https://doi.org/https://doi.org/10.1016/j.jinorgbio.2006.07.019.

[11] A.H. Calvert, S.J. Harland, D.R. Newell, Z.H. Siddik, A.C. Jones, T.J. McElwain, S. Raju, E. Wiltshaw, I.E. Smith, J.M. Baker, M.J. Peckham, K.R. Harrap, Early clinical studies with cis-diammine-1,1-cyclobutane dicarboxylate platinum II, Cancer Chemother. Pharmacol. 9 (1982) 140–147. https://doi.org/10.1007/BF00257742.

[12] K.S. Egorova, V.P. Ananikov, Toxicity of Metal Compounds: Knowledge and Myths, Organometallics. 36 (2017) 4071–4090. https://doi.org/10.1021/acs.organomet.7b00605.

[13] L. Jin, C. Quan, X. Hou, S. Fan, Potential Pharmacological Resources: Natural Bioactive Compounds from Marine-Derived Fungi, Mar. Drugs. 14 (2016). https://doi.org/10.3390/md14040076.

[14] K. Trisuwan, V. Rukachaisirikul, Y. Sukpondma, S. Preedanon, S. Phongpaichit, J. Sakayaroj, Pyrone derivatives from the marine-derived fungus Nigrospora sp. PSU-F18, Phytochemistry. 70 (2009) 554–557. https://doi.org/10.1016/j.phytochem.2009.01.008.

[15] T. Zhao, L.L. Xu, Y. Zhang, Z.H. Lin, T. Xia, D.F. Yang, Y.M. Chen, X.L. Yang, Three new α-pyrone derivatives from the plant endophytic fungus Penicillium ochrochloronthe and their antibacterial, antifungal, and cytotoxic activities, J. Asian Nat. Prod. Res. 21 (2019) 851–858. https://doi.org/10.1080/10286020.2018.1495197.

[16] C. Yuan, H.X. Yang, Y.H. Guo, L. Fan, Y.B. Zhang, G. Li, New α-pyrones from an endophytic fungus,: Hypoxylon investiens J2, RSC Adv. 9 (2019) 27419–27423. https://doi.org/10.1039/c9ra05308e.

[17] A.P.G. Macabeo, A.J.C. Cruz, A. Narmani, M. Arzanlou, A. Babai-Ahari, L.A.E. Pilapil, K.Y.M.

Garcia, V. Huch, M. Stadler, Tetrasubstituted α-pyrone derivatives from the endophytic fungus, Neurospora udagawae, Phytochem. Lett. 35 (2020) 147–151. https://doi.org/10.1016/j.phytol.2019.11.010.

[18] D. Lai, Z. Mao, Z. Zhou, S. Zhao, M. Xue, J. Dai, L. Zhou, D. Li, New chlamydosporol derivatives from the endophytic fungus Pleosporales sp. Sigrf05 and their cytotoxic and antimicrobial activities, Sci. Rep. 10 (2020) 8193. https://doi.org/10.1038/s41598-020-65148-0.

[19] S. Amatori, G. Ambrosi, M. Fanelli, M. Formica, V. Fusi, L. Giorgi, E. MacEdi, M. Micheloni, P. Paoli, R. Pontellini, P. Rossi, Synthesis, basicity, structural characterization, and biochemical properties of two [(3-hydroxy-4-pyron-2-yl)methyl]amine derivatives showing antineoplastic features., J. Org. Chem. 77 (2012) 2207–2218. https://doi.org/10.1021/jo202270j.

[20] S. Amatori, I. Bagaloni, E. MacEdi, M. Formica, L. Giorgi, V. Fusi, M. Fanelli, Malten, a new synthetic molecule showing in vitro antiproliferative activity against tumour cells and induction of complex DNA structural alterations, Br. J. Cancer. 103 (2010) 239–248. https://doi.org/10.1038/sj.bjc.6605745.

[21] A. Barve, A. Kumbhar, M. Bhat, B. Joshi, R. Butcher, U. Sonawane, R. Joshi, Mixed-ligand copper(II) maltolate complexes: Synthesis, characterization, DNA binding and cleavage, and cytotoxicity, Inorg. Chem. 48 (2009) 9120–9132. https://doi.org/10.1021/ic9004642.

[22] A. Otero-De-La-Roza, E.R. Johnson, A benchmark for non-covalent interactions in solids, J. Chem. Phys. 137 (2012). https://doi.org/10.1063/1.4738961.

[23] E. Stoler, J.C. Warner, Non-Covalent derivatives: Cocrystals and eutectics, Molecules. 20 (2015) 14833–14848. https://doi.org/10.3390/molecules200814833.

[24] A. Karshikoff, Non-covalent interactions in proteins, 2006. https://doi.org/10.1142/P477.

[25] J. Černý, P. Hobza, Non-covalent interactions in biomacromolecules, Phys. Chem. Chem. Phys. 9 (2007) 5291–5303. https://doi.org/10.1039/b704781a.

[26] S.U. Rehman, T. Sarwar, M.A. Husain, H.M. Ishqi, M. Tabish, Studying non-covalent drug-DNA interactions, Arch. Biochem. Biophys. 576 (2015) 49–60. https://doi.org/10.1016/j.abb.2015.03.024.

[27] K.D. Patel, U.H. Patel, Quantitative analysis of weak interactions by Lattice energy calculation, Hirshfeld surface and DFT studies of sulfamonomethoxine, J. Mol. Struct. (2017). https://doi.org/10.1016/j.molstruc.2016.08.046.

[28] D. Vashisht, S. Sharma, R. Kumar, V. Saini, V. Saini, A. Ibhadon, S.C. Sahoo, S. Sharma, S.K. Mehta, R. Kataria, Dehydroacetic acid derived Schiff base as selective and sensitive colorimetric chemosensor for the detection of Cu(II) ions in aqueous medium, Microchem. J. 155 (2020) 104705. https://doi.org/10.1016/j.microc.2020.104705.

[29] R. Kumar, V. Mutreja, G. Sharma, S. Kumar, A. Ali, S.K. Mehta, P. Venugopalan, R. Kataria, S.C. Sahoo, The role of a weakly coordinating thioether group in ligation controlled molecular self-assemblies and their inter-conversions in Ni(ii) complexes of l-methionine derived ligand, New J. Chem. 43 (2019) 11222–11232. https://doi.org/10.1039/c9nj02573a.

[30] G. Singh, J. Sindhu, Manisha, V. Kumar, V. Sharma, S.K. Sharma, S.K. Mehta, M.H. Mahnashi, A. Umar, R. Kataria, Development of an off-on selective fluorescent sensor for the detection of Fe3+ ions

based on Schiff base and its Hirshfeld surface and DFT studies, J. Mol. Liq. 296 (2019). https://doi.org/10.1016/j.molliq.2019.111814.

[31] X. Wang, H. Wang, P. Chen, Y. Pang, Z. Zhao, G. Wu, Synthesis and Biological Activities of Some Novel (E)-Alpha-(methoxyimino)benzeneacetate Derivatives with Modified 1,2,4-Triazole Moiety, J. Chem. 2014 (2014) 1–10. https://doi.org/10.1155/2014/681364.

[32] M.R. Maurya, N. Saini, F. Avecilla, Liquid phase versus microwave assisted selective oxidation of volatile organic compounds involving dioxidomolybdenum(VI) and oxidoperoxidomolybdenum(VI) complexes as catalysts in the presence/absence of an N-based additive, Polyhedron. 90 (2015) 221–232. https://doi.org/10.1016/j.poly.2015.01.030.

[33] A.L.S.I. Clinical, Document M27-A4, Ref. Method Broth Dilution Antifung. Suscetibility Test. Yeasts. (2012).

[34] CLSI, M38-A2 Reference Method for Broth Dilution Antifungal Susceptibility Testing of Filamentous Fungi; Approved Standard—Second Edition, Clin. Lab. Stand. Inst. 28 (2008) 29.

[35] B.L.Z. F. R. Cockerill, M. A. Wiker, J. Alder, M. N. Dudley, G. M. Eliopoulos, M. J. Ferraro, D. J. Hardy, D. W. Hecht, J. A. Hindler, J. B. Patel, M. Powell, J. M. Swenson, R. B. Thomson, M. M. Traczewski, J. D. Turnidge, M. P. Weinstein, Methods for Dilution Antimicrobial Susceptibility Tests for Bacteria That Grow Aerobically ; Approved Standard — Ninth Edition, 2012.

[36] Agilent, CrysAlisPro Data Collection and Processing Software for Agilent X-ray Diffractometers, Technol. UK Ltd, Yarnton, Oxford, UK. 44 (2014) 1–53.

[37] O. V. Dolomanov, L.J. Bourhis, R.J. Gildea, J.A.K. Howard, H. Puschmann, OLEX2: A complete structure solution, refinement and analysis program, J. Appl. Crystallogr. 42 (2009) 339–341. https://doi.org/10.1107/S0021889808042726.

[38] M.C. Burla, R. Caliandro, M. Camalli, B. Carrozzini, G.L. Cascarano, L. De Caro, C. Giacovazzo, G. Polidori, D. Siliqi, R. Spagna, IL MILIONE: A suite of computer programs for crystal structure solution of proteins, J. Appl. Crystallogr. 40 (2007) 609–613. https://doi.org/10.1107/S0021889807010941.

[39] G.M. Sheldrick, Crystal structure refinement with SHELXL, Acta Crystallogr. Sect. C Struct. Chem. 71 (2015) 3–8. https://doi.org/10.1107/S2053229614024218.

[40] A.D. Becke, Density-functional thermochemistry. I. The effect of the exchange-only gradient correction, J. Chem. Phys. 96 (1992) 2155–2160. https://doi.org/10.1063/1.462066.

[41] A.C. Ekennia, A.A. Osowole, L.O. Olasunkanmi, D.C. Onwudiwe, O.O. Olubiyi, E.E. Ebenso, Synthesis, characterization, DFT calculations and molecular docking studies of metal (II) complexes, J. Mol. Struct. 1150 (2017) 279–292. https://doi.org/10.1016/j.molstruc.2017.08.085.

[42] A.W. Addison, T.N. Rao, Synthesis, Structure, and Spectroscopic Properties, Dalt. Trans. (1984) 1349–56.

[43] U. Kendur, G.H. Chimmalagi, S.M. Patil, K.B. Gudasi, C.S. Frampton, Synthesis, structural characterization and biological evaluation of mononuclear transition metal complexes of zwitterionic dehydroacetic acid N-aroylhydrazone ligand, Appl. Organomet. Chem. 32 (2018) 1–21. https://doi.org/10.1002/aoc.4278.

[44] U. Kendur, G.H. Chimmalagi, S.M. Patil, K.B. Gudasi, C.S. Frampton, C. V. Mangannavar, I.S. Muchchandi, Mononuclear late first row transition metal complexes of ONO donor hydrazone ligand: Synthesis, characterization, crystallographic insight, in vivo and in vitro anti-inflammatory activity, J. Mol. Struct. 1153 (2018) 299–310. https://doi.org/10.1016/j.molstruc.2017.10.022.

[45] M.A. Spackman, D. Jayatilaka, Hirshfeld surface analysis, CrystEngComm. (2009). https://doi.org/10.1039/b818330a.

[46] F.P.A. Fabbiani, L.T. Byrne, J.J. McKinnon, M.A. Spackman, Solvent inclusion in the structural voids of form II carbamazepine: single-crystal X-ray diffraction, NMR spectroscopy and Hirshfeld surface analysis, CrystEngComm. 9 (2007) 728–731. https://doi.org/10.1039/B708303N.

[47] G.A. Stephenson, E.G. Groleau, R.L. Kleemann, W. Xu, D.R. Rigsbee, Formation of Isomorphic Desolvates: Creating a Molecular Vacuum, J. Pharm. Sci. 87 (1998) 536–542. https://doi.org/https://doi.org/10.1021/js970449z.

[48] P.W. Ayers, M. Levy, Perspective on "Density functional approach to the frontier-electron theory of chemical reactivity," Theor. Chem. Acc. 103 (2000) 353–360. https://doi.org/10.1007/s002149900093.

[49] P.K. Chattaraj, Chemical Reactivity and Selectivity: Local HSAB Principle versus Frontier Orbital Theory, J. Phys. Chem. A. 105 (2001) 511–513. https://doi.org/10.1021/jp003786w.

[50] A.H. Delcour, Outer membrane permeability and antibiotic resistance, Biochim. Biophys. Acta - Proteins Proteomics. 1794 (2009) 808–816. https://doi.org/https://doi.org/10.1016/j.bbapap.2008.11.005.

Graphical Abstract

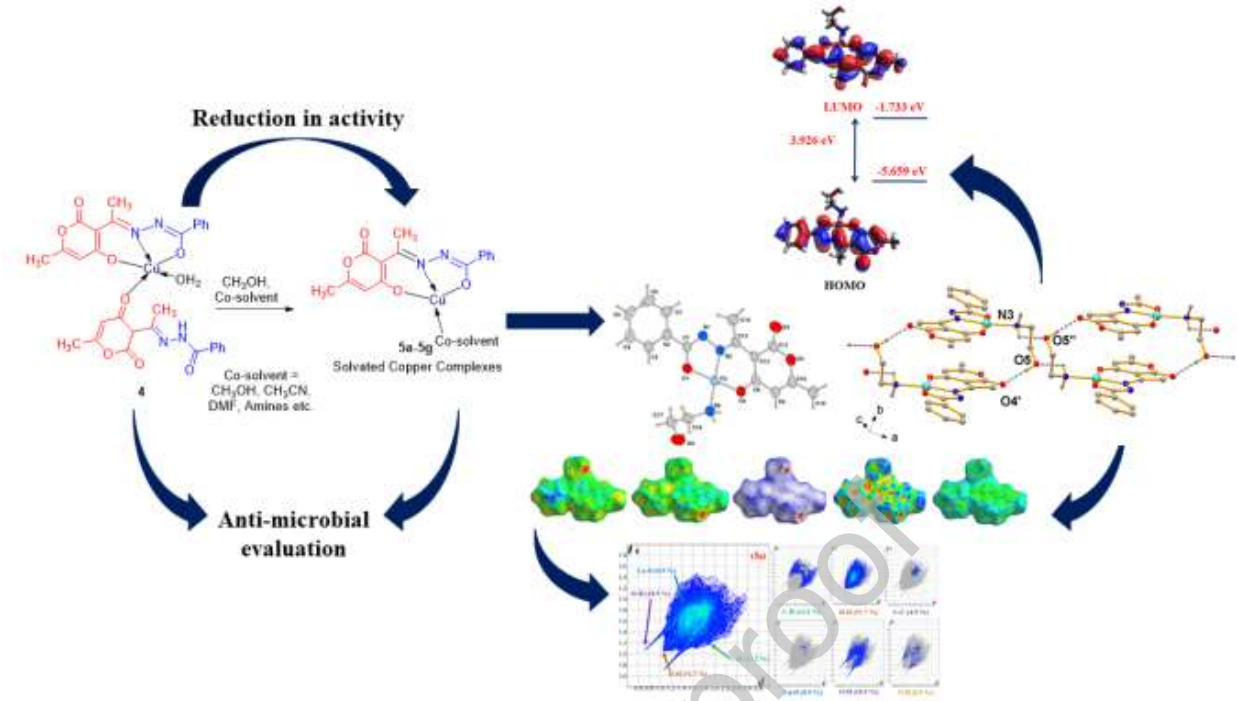

A series of novel solvent coordinated copper(II) complex with hydrazone of 3-acetyl-6-methyl-2*H*-pyran-2,4(3*H*)-dione (DHA) have been synthesized. Structural aspects, electrostatic and biological properties related with these complexes have been studied.